

**OPEN ACCESS**

## Numerical modelling of plasma spray process

To cite this article: K Ramachandran 2010 *J. Phys.: Conf. Ser.* **208** 012052

View the [article online](#) for updates and enhancements.

### Related content

- [Modelling of non-transferred argon-nitrogen plasma arc and plasma jet](#)  
B Selvan, K Ramachandran, T K Thiyagarajan et al.
- [Three-dimensional effects of carrier gas and particle injections on the thermo-fluid fields of plasma jets](#)  
Kandasamy Ramachandran and Hideya Nishiyama
- [Modelling of arc behaviour inside a F4 APS torch](#)  
K Ramachandran, J-L Marqués, R VaBen et al.

### Recent citations

- [Numerical simulation study on fluid dynamics of plasma window using argon](#)  
S. Huang *et al*
- [Carbothermal reduction of sillimanite in a transferred arc thermal plasma reactor](#)  
M. Vijay *et al*



**ECS** **240th ECS Meeting**  
Oct 10-14, 2021, Orlando, Florida

**Register early and save up to 20% on registration costs**

Early registration deadline Sep 13

**REGISTER NOW**

## Numerical modelling of plasma spray process

**K Ramachandran**

School of Mechanical and Building Sciences,  
VIT University, Vellore- 632014, India

E-mail: kramachandran@vit.ac.in

**Abstract:** Reproduction of the coating quality in the plasma spraying is tough task. To overcome this problem, it is necessary to understand the behaviour of the arc inside the torch, plasma jet and particles in a plasma jet. Various experimental and modelling works have been carried out on these topics. In this article, a few of our new results of plasma arc inside the torch are presented and some of our simulated results of plasma jets and particle behaviour in a plasma jet are summarized. Electro-thermal efficiencies predicted using two different models are close to the measured one. The effect of atmosphere, where the plasma jet is issued, on temperature field is stronger than on velocity field. The influence of the carrier gas and particle loading on the plasma jet thermo-fluid fields is discussed. The effects of particle loading and turbulence modulation on the particle velocity and temperature are clarified. Turbulence modulation does not affect the particle dispersion significantly.

### 1. Introduction

Plasma spraying, one of the coating techniques in the family of thermal spraying, is used to coat metals, alloys, ceramic, cermets, and plastic etc. In the plasma spray process, an electric arc is generated between conical shape cathode made up of thoriated tungsten and cylindrical shape anode nozzle made up of copper. When an injected plasma forming gas passes through an arc, the same is ionized and plasma plume come out from the nozzle. The plasma jet has large temperature and velocity gradients both in radial and axial directions. Coating material is injected into the plasma jet perpendicular to torch axis. Injected powder particles get momentum and energy from the plasma and molten particles are projected on the substrate, where the coating is formed.

Although plasma spraying has been used for long time, reproduction of the coating quality is very difficult task. Quality of the coating is strongly influenced by an arc fluctuation inside the torch, plasma-particles interaction process and formation of the coating on the substrate. In order to control quality of the coatings, a complete knowledge on these processes must be acquired. Numerous research works [ex. 1-16] have been carried out to study these processes. Experimental works [ex. 3, 8, 15] on these topics are limited by an involvement of high cost equipments and measurement difficulties. Numerical modelling and simulation of these processes help to understand the physics involved in the same. Various two-dimensional [ex. 9, 13, 17-19] and three-dimensional [ex. 4-6, 20-22] models have been developed to simulate an arc and plasma-particles interaction. Since the arc attaches at small area of the anode nozzle, plasma flow has three-dimensional effects inside the nozzle as well as at the nozzle exit. Since particles are injected into the plasma jet through a single port, plasma-particles interaction produces three-dimensional effects in the plasma jet. Hence two-dimensional models could not predict the realistic situation takes place inside the torch and in a plasma

jet. In this paper, some of our three-dimensional model results of behaviour of an arc inside the torch, plasma jet and particles in a plasma jet are summarized.

## 2. Model description

A simplified form of governing equations to simulate plasma arc and plasma-particles interaction is as follows.

$$\text{div}(\rho \mathbf{V} \phi) - \text{div}(\Gamma_{\phi} \text{grad } \phi) = S_{\phi} \quad (1)$$

where  $\rho$ ,  $\mathbf{V}$ ,  $\phi$ ,  $\Gamma_{\phi}$  and  $S_{\phi}$  are density, velocity vector, solved / dependent variable, exchange coefficient and source term respectively.

### 2.1. Plasma arc

The assumptions used to develop three-dimensional model to simulate the plasma arc are

- Plasma flow is steady, laminar and incompressible.
- Plasma is in local thermodynamic equilibrium (LTE) and optically thin.
- Non-LTE at the vicinity of the cold cathode and anode is not considered.
- Arc core radius ( $R_{\text{arc}}$ ) is a radial distance along the cathode from the centreline to the point at which current density is zero.
- Arc length ( $L_{\text{arc}}$ ) is an axial distance from the cathode to the centre point of the anode arc spot.

The governing equations to be solved to simulate the plasma arc are continuity, momentum (in three directions) and energy. In addition to flow and energy equations, electric potential and vector potential (in three directions) equations without convection term are solved to account electromagnetic effects. Information regarding the computational domain and boundary conditions to simulate an arc inside the plasma torch can be obtained from [4-5]. All the governing equations that can be derived from equation (1) by substituting appropriate  $\phi$ ,  $\Gamma_{\phi}$  and  $S_{\phi}$ , are solved simultaneously with necessary boundary conditions using SIMPLE algorithm formulated in commercial CFD software FLUENT 6.3.

As a first step, the size of the anode arc spot at the anode wall is assumed to be equal to the size of the arc core at the cathode. Since there is no experimental data on the size of the anode spot to use it, this poor assumption is justified. At the anode spot and wall, electric potential and gradient of electric potential are assumed to zero respectively. Heat flux to the anode wall due to electron condensation, electron enthalpy transport, radiation and conduction is given by [14, 23-24]

$$Q_a = j\phi_w + \frac{5k_B}{2e} jT - \lambda \left. \frac{\partial T}{\partial r} \right|_{\text{wall}} + S_R = h_{\text{conv}}(T_{\text{wall}} - T_{\text{water}}) \quad (2)$$

Here  $\phi_w$ ,  $k_B$ , and  $e$  are the work function of the anode material, Boltzmann's constant and the electron charge respectively. Since plasma is optically thin, it is assumed that radiation energy ( $S_R$ ) lost by the plasma is observed by the torch wall. Heat flux to the anode wall due to ion recombination is neglected since their contribution is about 5% of the total heat flux to the anode [23-24]. The radiation from the wall is also negligible since entire wall has a temperature of 300K except arc spot. The convective heat transfer coefficient of cooling water  $h_{\text{conv}}$  is assumed as  $2.0 \times 10^5 \text{ W/m}^2\text{K}$  [5,6,14].  $T_{\text{wall}}$  and  $T_{\text{water}}$  are respectively the local temperature of the wall and the temperature of the cooling water (300 K).

### 2.2. Plasma jet and plasma-particles interaction

The following assumptions are used to develop three-dimensional models to simulate the plasma jet and plasma-particles interaction process.

- Plasma flow is steady, in local thermodynamic equilibrium (LTE), optically thin, turbulent and incompressible.
- Particle loading is dilute.

- Temperature gradient within the particle, radiation from the particles and interaction between particles are not considered.
- Computational particles are used instead of real particles.

To simulate the plasma jet, continuity, momentum (in three directions), energy, species, kinetic energy and dissipation rate equations are derived by incorporating appropriate  $\phi$ ,  $T_\phi$  and  $S_\phi$  in equation (1). Standard K- $\epsilon$  model [22] is used to take into account the turbulent characteristics of the plasma jet.

Details of the computational domain and boundary conditions are found in [22, 26, 27]. Boundary conditions at the nozzle exit are assumed either from global mass-energy relation [10] or from experimental data [25]. The velocity and temperature profiles at the nozzle exit are as follows

$$w = w_{\max}[1 - (Y/R_0)^n] \quad (3)$$

$$T = (T_{\max} - T_{\text{wall}})[1 - (Y/R_0)^m] + T_{\text{wall}} \quad (4)$$

Here  $w$ ,  $w_{\max}$ ,  $T$ ,  $T_{\max}$ ,  $T_{\text{wall}}$ ,  $Y$  and  $R_0$  are axial velocity, maximum axial velocity/axial velocity at the centre point, temperature, maximum temperature/ temperature at the centre point, wall temperature, radial distance and nozzle radius respectively. The appropriate values of  $n$ ,  $m$  are chosen to match the effective power of the plasma that coming out from the nozzle exit. Generally the radial velocity at the nozzle exit is assumed to be zero. The SIMPLEST algorithm is used to solve the governing equations through PHOENICS CFD code.

Lagrangian equation of motion and heat balance equation are used to simulate the particle behaviour in a plasma jet [22,26,27]. The position of the particle is determined from its velocity. The drag coefficient is corrected by a factor, which accounts the variable property effect [22,26,27].The effect of turbulence on the particles is simulated by a stochastic model [22,26,27] in which particles are assumed to be deflected by the eddies when they cross. The temperature of the particle is determined from the solution of the heat balance equation neglecting the radiation effects. Nusselt number used to calculate the particle heat transfer coefficient is corrected by two factors, which account the variable property effect. In the plasma-particle interaction process, exchange of momentum, energy, turbulence can not be neglected especially when particle loading dilute or dense. Hence two-way interaction sources [22] are added in the governing equations of the plasma jet. In order to account the turbulence modulation in the carrier phase (plasma jet), the extensions [28] are incorporated in the standard K- $\epsilon$  model. In this model, the volume fraction of the plasma in each cell is approximated to unity. This assumption may be valid since the volume fraction of the particles in each cell is less than 0.01 in the present study (dilute particle loading).

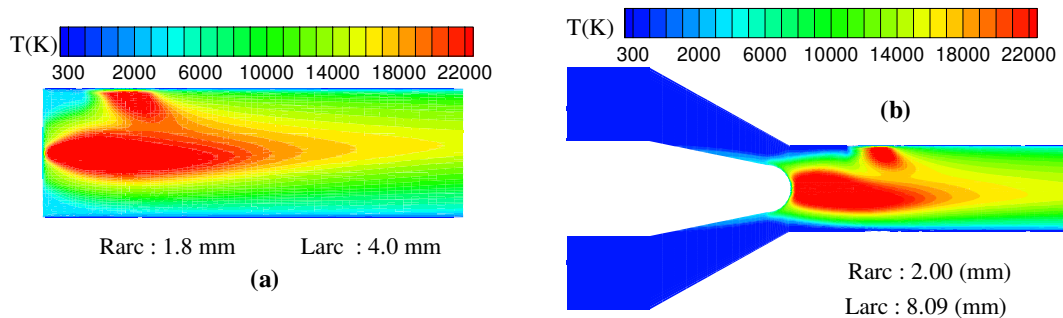
In the present work, computational particles, which are representative of group of similar particles, are used instead of real particles. Ten or twenty computational particles are used for the calculation. Steel particles of size 20-40  $\mu\text{m}$  are transversely injected with an injection velocity of 12.0 m/s. Heat conduction inside the particles is not considered due to low Biot number. Since the non-continuum effect, Basset history term, and thermophoresis have no appreciable influence on particles behaviour with a size between 10  $\mu\text{m}$  and 100  $\mu\text{m}$  [19], they are not considered in this model. In the present calculations, the maximum particle loading ratio (particle mass flow rate / plasma gas mass flow rate) is less than 0.05. Hence, radiation from the plasma to particles as well as radiative exchange among the particles are neglected [29]. Smaller particle size, low particle surface temperature (< 2000 K) and high enthalpy difference between the plasma and surface of the particles except at the tail flame are the factors [29] to be able to neglect the radiative heat losses from the particles in this model.

### 3. Results and discussion

#### 3.1. Plasma arc

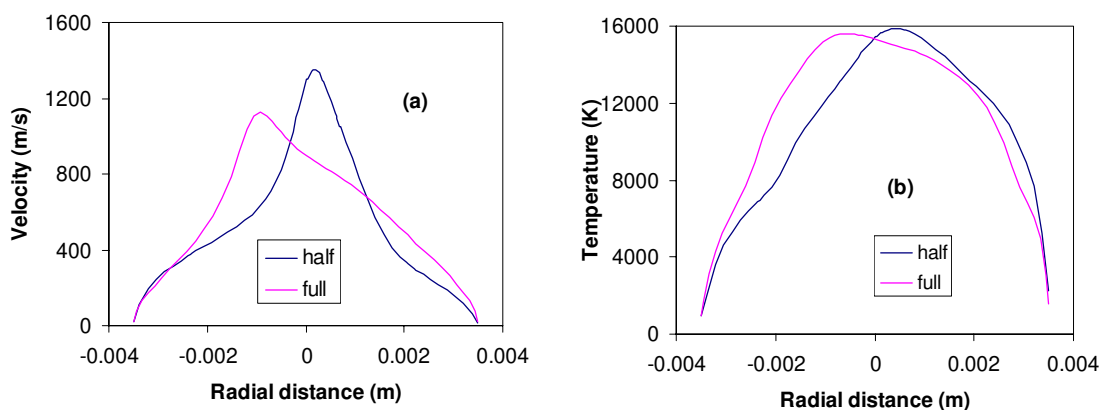
Experiments are conducted for gas flow rates of 20 slpm of Ar and 3 slpm of  $\text{N}_2$  and current of 500 A. The measured power and electro-thermal efficiency of the torch are 21.35 kW and 48.8 % respectively. The same input variables are used for the simulation. There are two models named as half-geometry model and full-geometry model used for the simulation. Half-geometry model ignores the cathode geometry whereas full-geometry model considers both cathode and anode geometries.

Temperature fields inside the plasma torch for 21.35 kW predicted from half-geometry and full-geometry models are shown in figure 1 (a) and (b) respectively. The arc radius and arc length, which can generate the power of 21.35 kW are mentioned in the figure 1 (a) and (b).



**Figure 1.** Temperature inside the plasma torch predicted from (a) half-geometry model and (b) full-geometry model

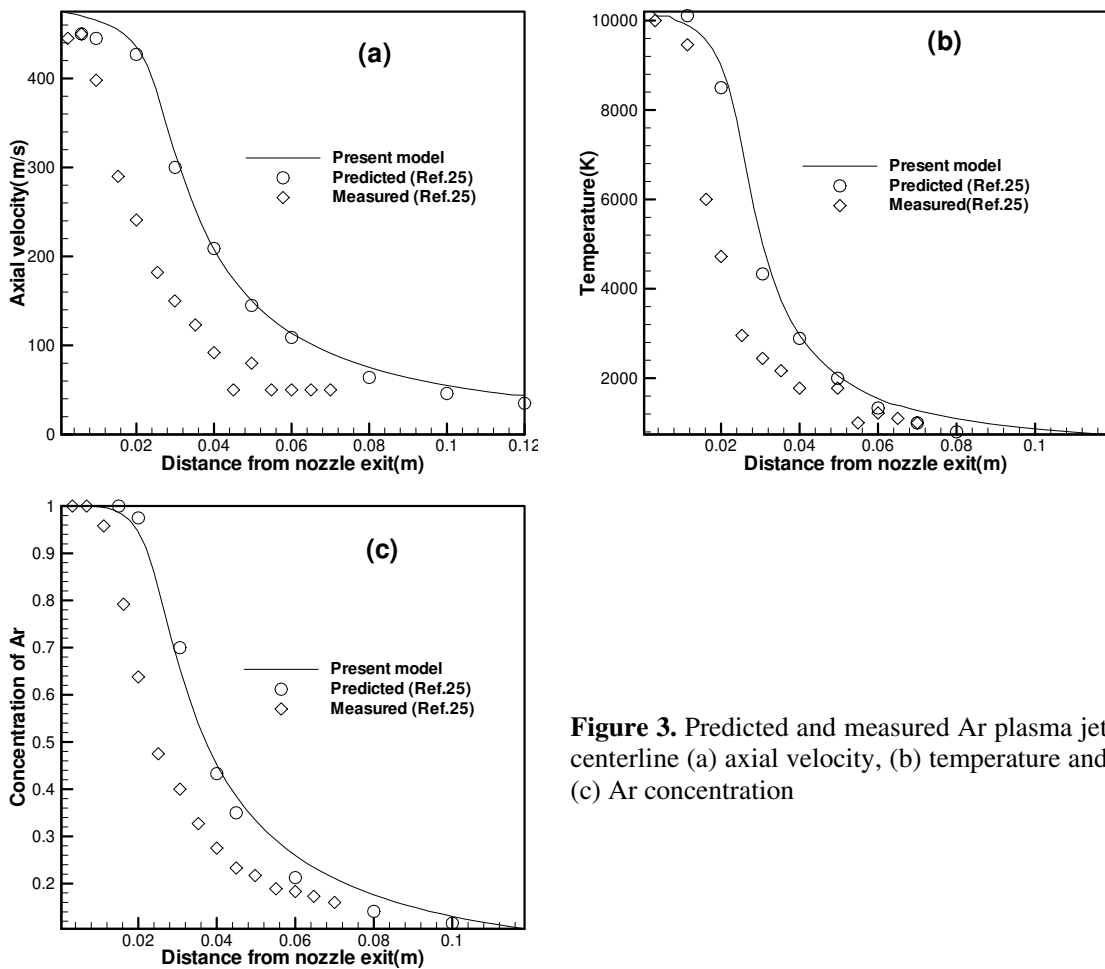
In both cases, arc radius is comparable but arc length in the full-geometry model is twice of the same predicted in the half-geometry model. This is because arc length ( $L_{arc}$ ) is assumed as an axial distance from the cathode at which current density is zero to the distance at which the centre of the anode arc spot at the wall in the full-geometry model whereas the same is assumed as an axial distance from the cathode tip/inlet to the distance at which the centre of the anode arc spot at the wall in the half-geometry model. Predicted electro-thermal efficiencies of the plasma torch using half- geometry and full-geometry models are 49 % and 46.3 % respectively. Half geometry model predicts electro-thermal efficiency very close to the experimental value. Also, electro-thermal efficiency predicted using full geometry model is comparable with measured one.



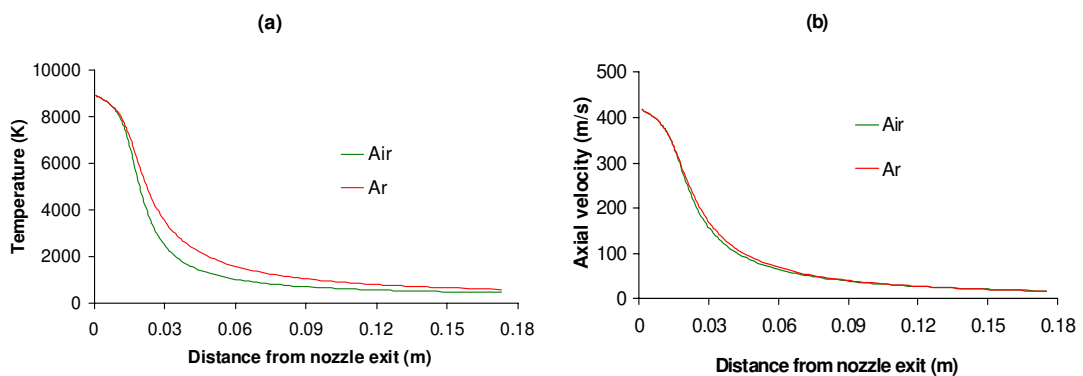
**Figure 2.** Nozzle exit (a) velocity and (b) temperature predicted from two different models.

Figure 2 shows nozzle exit (a) velocity and (b) temperature predicted from both half-geometry and full-geometry models. Three-dimensional effect is seen in both velocity and temperature fields. There is a small difference between temperature fields obtained from both models whereas large difference is seen between velocity fields obtained from both models. However, this effect is predominant in the plasma jet very close to the nozzle exit. If the particle is injected externally, both the parabolic profile

assumed at the nozzle exit and predicted nozzle exit profiles to simulate the plasma jet may have the same effect on particle behaviour.



**Figure 3.** Predicted and measured Ar plasma jet centerline (a) axial velocity, (b) temperature and (c) Ar concentration



**Figure 4.** Centreline (a) temperature and (b) axial velocity of the argon plasma jet issued into argon and air atmospheres.

### 3.2. Plasma jet and plasma-particles interaction

Predicted axial velocity, temperature and argon mass fraction of the argon plasma jet issued into the air atmosphere are compared with previous numerical and experimental results [25] in figure 3 a, b and c respectively. Present model assumes the values of  $T_{max}$ ,  $T_{wall}$ ,  $w_{max}$ ,  $n$  and  $m$  in the equations (3) and (4) are 10200 K, 500 K, 475 m/s, 3.2 and 4.1 respectively [25]. Results of present model are comparable with measurements. Also present model predicts axial velocity, temperature and argon mass fraction better than previous model. Figure 4 (a) and (b) show the centreline temperature and velocity of an argon plasma jet issued in to two different atmospheres (argon and air) respectively. Since the plasma jet is issued into cold atmosphere, both temperature and velocity of an argon jet are decreased along the axial direction. Also the temperature and velocity of the plasma jet issued into air are lower than that of same issued into argon. This is because momentum and thermal diffusion coefficients of the argon-air mixture are larger than that of argon. Since the Prandtl number of the argon-air mixture is less than unity, this effect is weaker on velocity than on temperature. This effect is not visible near the nozzle exit and in the downstream. The reason for the same is the mass fraction of the air near the nozzle exit is lower whereas the mass fraction of argon in the downstream is lower.

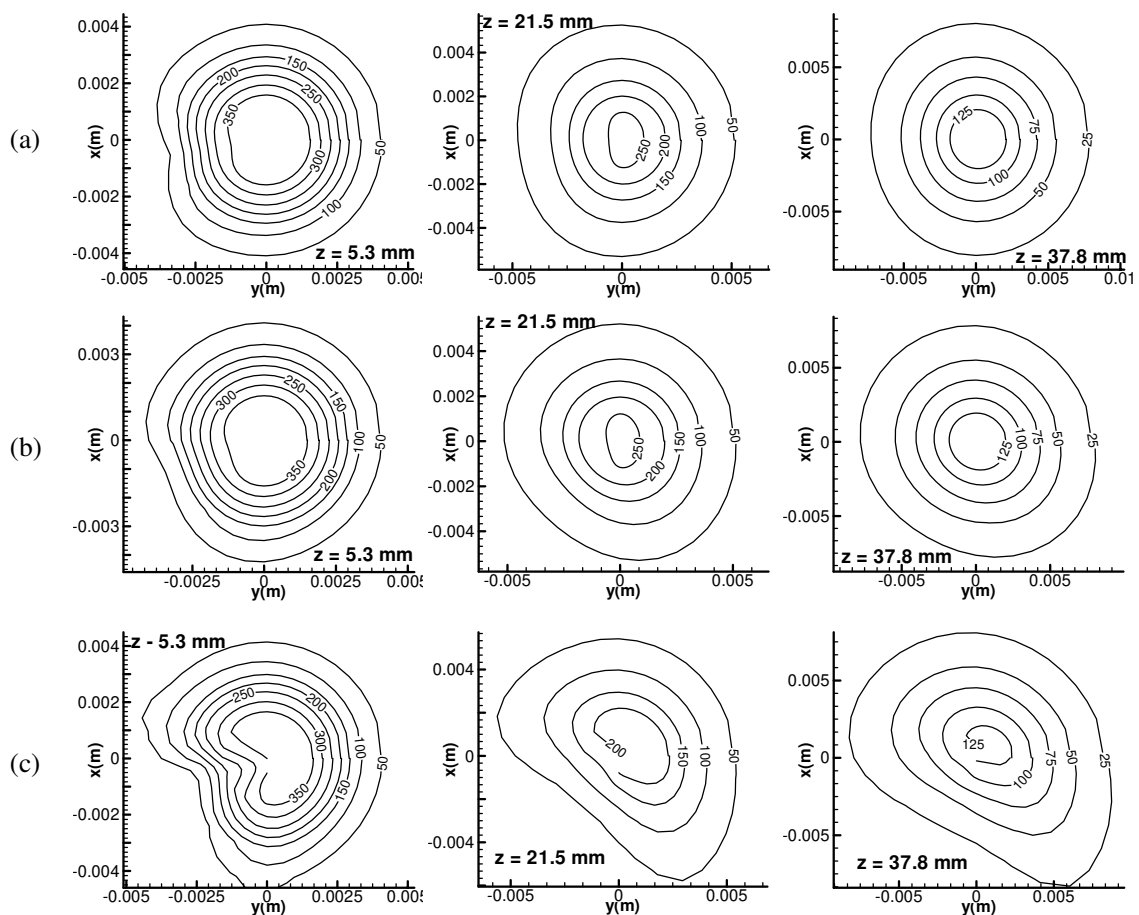


**Figure 5.** Effect of carrier gas on velocity field [m/s] of the plasma jet (a) without swirl ( $F_c = 0.064F_g$ ), (b) with swirl ( $u_{max} = 0.1w_{max}$  and  $F_c = 0.064F_g$ ) and (c) with swirl ( $u_{max} = 0.1w_{max}$  and  $F_c = 0.128F_g$ )

The effect of carrier gas on velocity and temperature fields of the argon plasma jet with and without swirl is shown in figures 5 and 6. In this case [26], argon jet is issued into argon atmosphere,

carrier gas is argon and maximum swirl velocity ( $u_{\max}$ ) of the swirl jet is 10 % of maximum axial velocity at the nozzle exit.  $F_c$  and  $F_g$  are mass flow rates of carrier and plasma gases respectively. At a lower carrier gas mass flow rate ( $F_c = 0.064F_g$ ), plasma jet fields are affected only at the carrier gas injection side (figures 5 (a) and 6 (a)). The deformation (figures 5 (b) and 6 (b)) caused by the same carrier gas mass flow rate on the swirl jet fields is different from that of plasma jet without swirl. Because of the azimuthal momentum, the deformation is rotated anti-clockwise. At a higher carrier gas mass flow rate ( $F_c = 0.128F_g$ ), the swirl jet fields are strongly affected including the core region as shown in figures 5(c) and 6(c). In all cases, the effect of carrier gas decreases in the downstream and the temperature field is more sensitive to the carrier gas than velocity field.

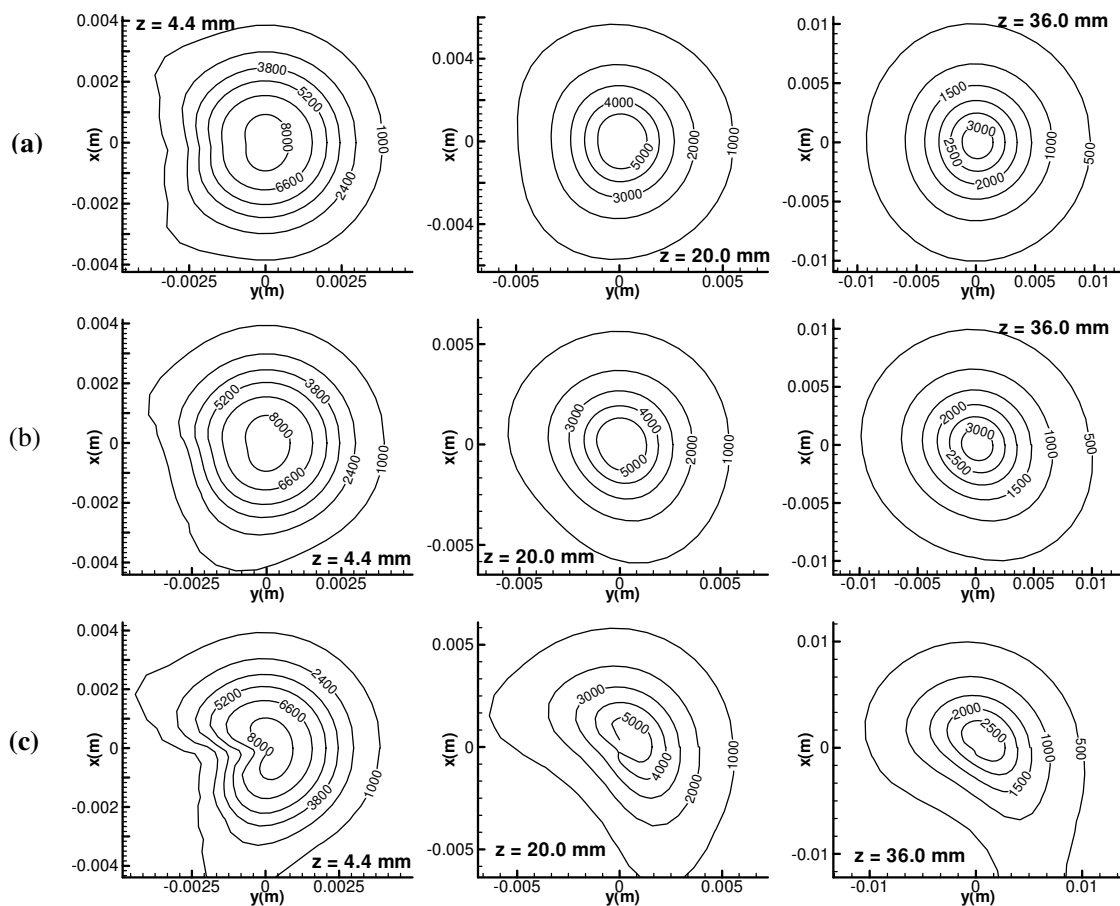


**Figure 6.** Effect of carrier gas on temperature field [K] of the plasma jet (a) without swirl ( $F_c = 0.064F_g$ ), (b) with swirl ( $u_{\max} = 0.1w_{\max}$  and  $F_c = 0.064F_g$ ) and (c) with swirl ( $u_{\max} = 0.1w_{\max}$  and  $F_c = 0.128F_g$ )

Figures 7 and 8 show the effect of particle loading on velocity and temperature fields of the plasma jet respectively. In this case [26], particles are injected into argon plasma jet (without swirl) with carrier gas. Mass flow rate of the carrier gas (argon) is 6.4%  $F_g$  and particle turbulent dispersion is considered. Since the particles are dispersed in the plasma jet, they have different trajectories and total mass of the injected particles are distributed. The momentum and energy transfers follow the particle trajectories. There is no appreciable difference on local deformation on velocity and temperature fields between particle loading of  $0.5 \text{ kg h}^{-1}$  and  $1.0 \text{ kg h}^{-1}$ . The total momentum and energy transfers are higher but specific momentum and energy transfers are lower at higher particle loading. For example,



5.79 % of the plasma jet input axial momentum is transferred to the particles at the particle loading  $0.5 \text{ kg h}^{-1}$  whereas at the particle loading  $1.0 \text{ kg h}^{-1}$ , 6.56 % of the same is transferred to the particles. At higher particle loading, the deformation of the thermo-fluid fields is relaxed slowly. The velocity field is more sensitive to the particle loading than temperature field especially at the particle injection region and total momentum transfer is larger than total energy transfer between plasma and particles.

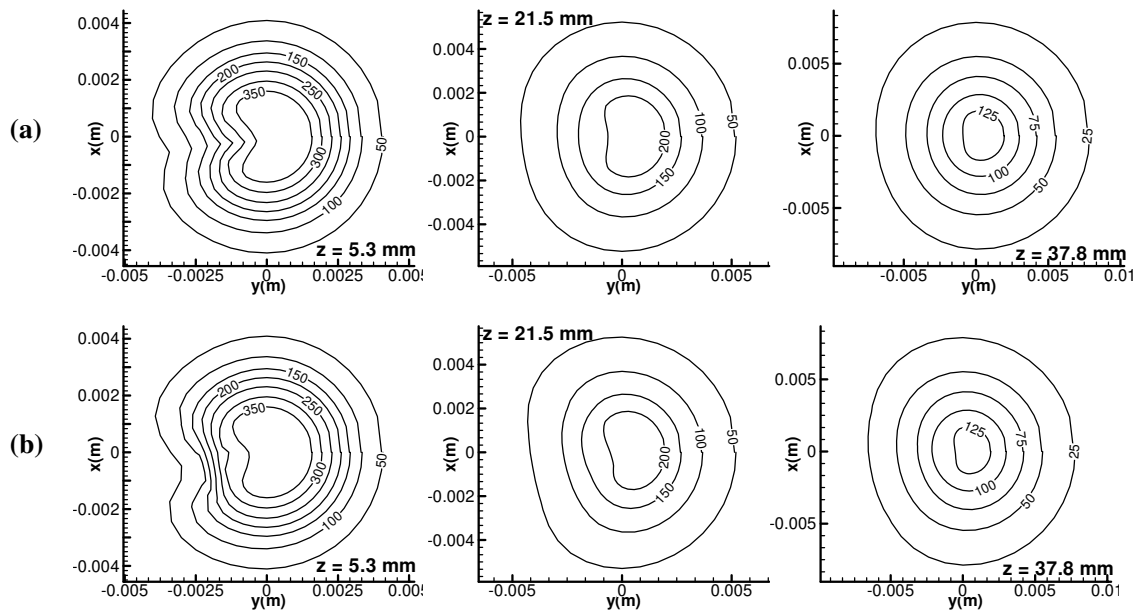


**Figure 7.** Influence of the particle loading on velocity field [m/s] of the plasma jet without swirl including the particle turbulent dispersion (a)  $0.5 \text{ kg h}^{-1}$  and (b)  $1.0 \text{ kg h}^{-1}$

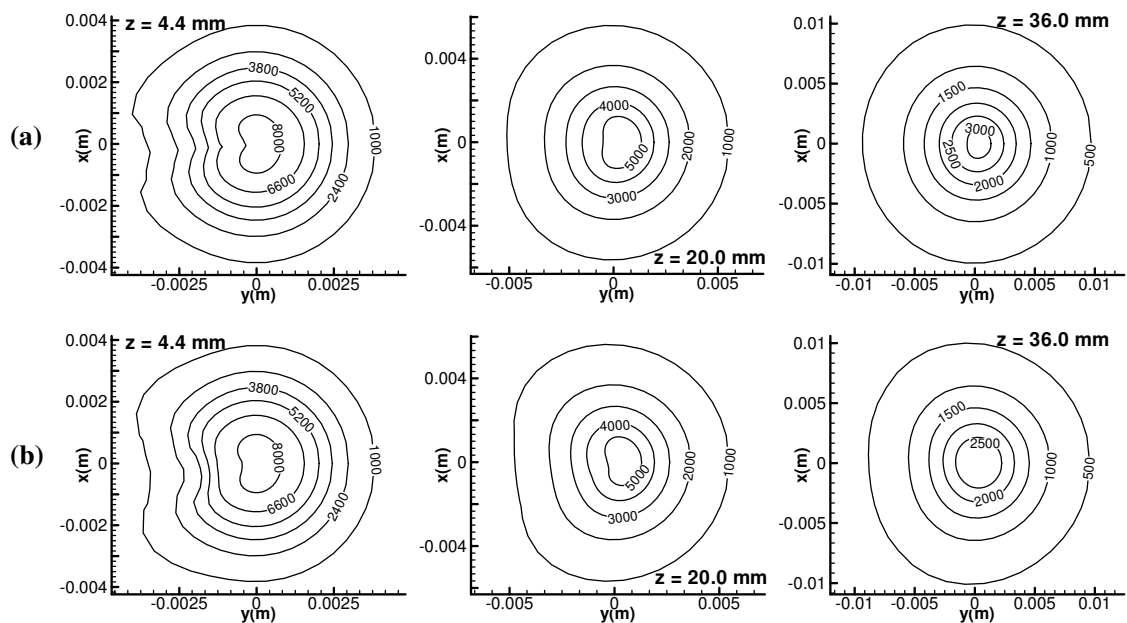


**Figure 8.** Temperature field [K] of the plasma jet without swirl including the particle turbulent dispersion for different particle loadings (a)  $0.5 \text{ kg h}^{-1}$  and (b)  $1.0 \text{ kg h}^{-1}$

To validate the plasma-particles interaction model, particle velocity and temperature are compared with both experimental and previous model results [16]. In this case, NiCrAlY particle is injected into Ar-H<sub>2</sub> plasma jet issued into air atmosphere. Both velocity (figure 9 (a)) and temperature (figure 9 (b)) of the particle show satisfactory agreement with experimental results. The difference between predicted and experimental results is mainly due to the assumption of thermo-physical properties of Ni for NiCrAlY particle.

Figure 10 (a) and (b) show the particle velocity and temperature respectively for two different particle loadings at various axial distances in an argon plasma jet issued into air atmosphere. Exchange of momentum and energy between plasma and particles and effect of turbulence of the jet on the particles are considered [27]. Steel particles of size 20  $\mu\text{m}$  are injected externally through a carrier gas. At higher particle loading (1.0 kg/h), distributions of both particle temperature and velocity are wider than at lower particle loading (0.5 kg/h) along the axial distance. Very low particle temperature and velocity are observed at particle loading 1.0 kg/h. This is because specific energy and momentum transfers at higher particle loading are lower than that at lower particle loading.

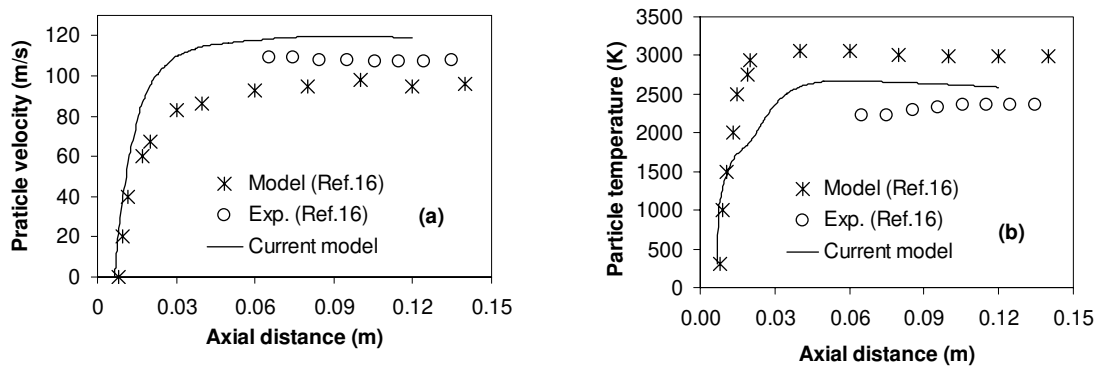


**Figure 9.** Particle (a) velocity and (b) temperature in an Ar-H<sub>2</sub> plasma jet

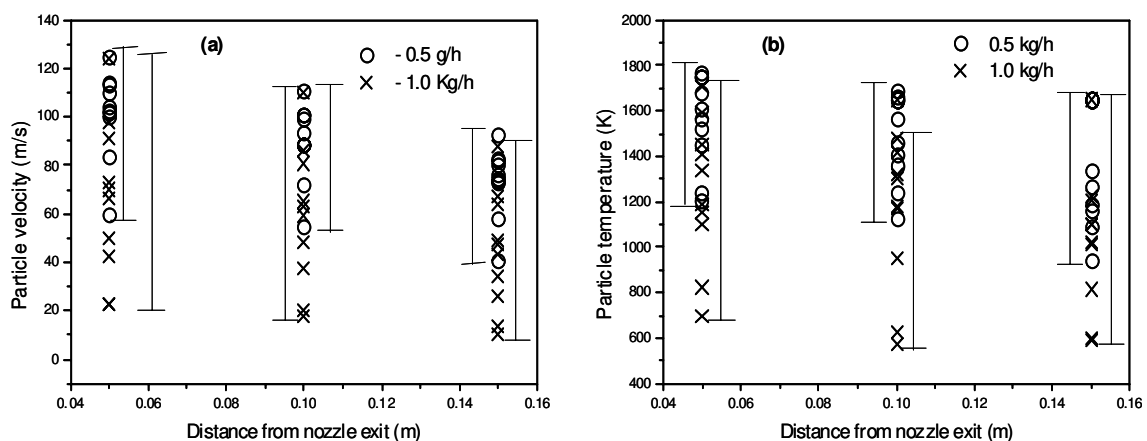


**Figure 10.** Particle (a) velocity and (b) temperature distributions along the axial distance for different particle loadings.

Generally, models of plasma-particles interaction consider the exchange of energy and momentum between plasma and particles and the effect of plasma jet turbulence on the particle dispersion.

Injected particles can modulate the turbulence of the plasma jet when the particle loading is dilute or dense. In order to develop a realistic model, two-way coupling of momentum, energy and turbulence between plasma and particles is considered [22]. Figure 11 (a) and (b) show particle temperature and velocity distributions respectively for with and without turbulence modulation at an axial distance of 12.0 cm. In this case, two-way interaction of energy and momentum between plasma and particles are considered. Both particle temperature and velocity distributions are narrower with turbulence modulation than without turbulence modulation. Range of particle temperature and velocity distributions decreases with increasing the particle size.

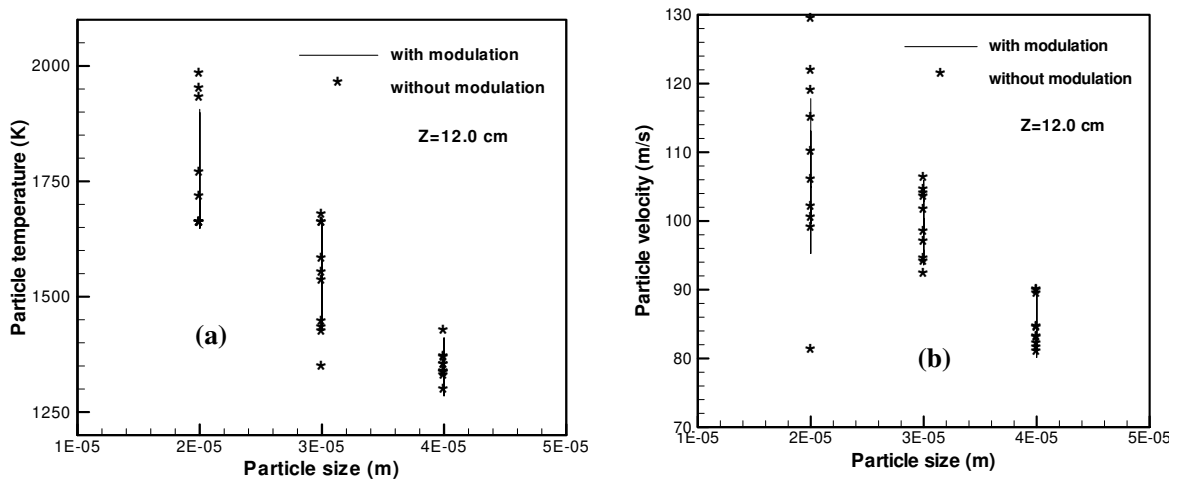


**Figure 11.** Particle (a) temperature and (b) velocity with and without turbulence modulation

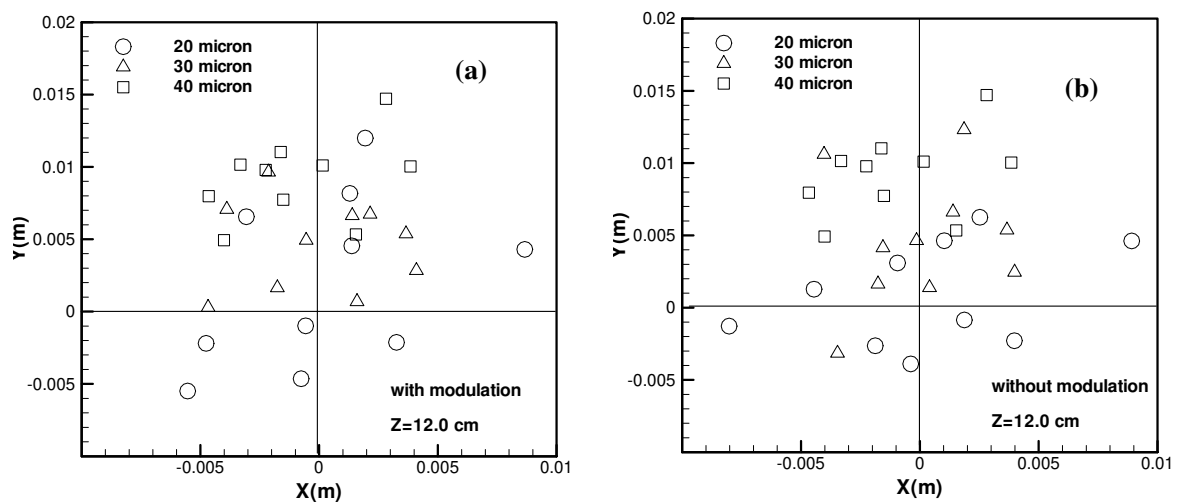


**Figure 12.** Particles dispersion (a) with and (b) without turbulent modulation

Figure 12 (a) and (b) show the particles dispersion in a plane at an axial distance of 12.0 cm with and without turbulent modulation respectively. Number of steel particles used here is ten. When turbulence modulation is considered, particles positions are changed a little from that without turbulence modulation. Smaller size particles are dispersed widely. Particles of 40  $\mu\text{m}$  are moved

away from the centreline whereas some of 20  $\mu\text{m}$  particles are not crossed the centreline. Larger particles can penetrate through the jet due to the higher inertial force. Since smaller particles do not have an adequate inertial force, they are deflected by the jet. The plasma input energy and axial momentum at the nozzle exit are 3.89 kW and 0.3 N respectively. In the fully coupled model, energy and momentum transfers are calculated when ten numbers of 25  $\mu\text{m}$  steel particles are injected. Energy and momentum transferred from plasma to particles are 0.912 % of input energy and 1.68 % of input momentum respectively [22]. Energy and momentum transfers decrease with increasing the particle size.

#### 4. Conclusion

Results of three-dimensional models used to simulate the plasma jet and plasma particles interaction process are reviewed and few new results of arc behaviour are discussed. The highlights of these studies are as follows.

Although, the difference between electro-thermal efficiencies predicted by half-geometry and full-geometry models is small, there is large difference between velocity fields at the nozzle exit predicted by these models. The effect of atmosphere, where the plasma jet is issued, on temperature and velocity of the plasma jet is significant and the same is stronger on temperature than on velocity. Carrier gas strongly deforms the plasma jet fields at higher mass flow rate whereas at lower mass flow rate, it affects only injection side of plasma jet fields. Temperature field is more sensitive to the carrier gas than velocity field. Velocity field is more sensitive to the particle loading than temperature field. At higher particle loading, total momentum and energy transfers are higher whereas specific momentum and energy transfers are lower. At higher particle loading, both particle temperature and velocity distributions are wider than at lower particle loading. Both particle temperature and velocity distributions are narrower with turbulence modulation than without turbulence modulation. Range of particle temperature and velocity distributions decreases with increasing the particle size. The effect of turbulence modulation on the particle dispersion is poor.

#### 5. References

- [1] Wutzke S A, Pfender E and Eckert E R G 1968 *AIAA J* **6** 1474
- [2] Duan Z and Heberlein J 2002 *J. Thermal Spray Technol.* **11** 44
- [3] Dorier J -L, Gindrat M, Hollenstein C, Salito A, Loch M and Barbezat G 2001 *IEEE Trans. Plasma Sci.* **29** 494
- [4] Trelles J P and Heberlein J V R 2006 *J. Thermal Spray Technol.* **15** 563
- [5] Ramachandran K, Marquès J -L, Vaßen R and Stöver D 2006 *J. Phys. D: Appl. Phys.* **39** 3323
- [6] Baudry C, Vardelle A and Mariaux G 2005 *High Technology Plasma Processes* **9** 1
- [7] Bolot R, Coddet C and Imbert M 1997 *Phoenics J. Comp. Fluid Dyn. Appl.* **10** 335
- [8] Spores R and Pfender E 1989 *Surf. Coat. Technol.* **37** 251
- [9] Murphy A B and Kovitya P 1993 *J. Appl. Phys.* **73** 4759
- [10] Chang C H and Ramshaw J. D 1993 *Plasma Chem. Plasma Process.* **13** 189
- [11] Wan Y P, Prasad V, Wang G. X, Sampath S and Finke J R 1999 *ASME J. Heat Transfer* **121** 691
- [12] Ahmed I and Bergman T L 2000 *J. Thermal Spray Technol.* **9** 215
- [13] Gonzalez J J, Fretton P and Gleizes A 2002 *J. Phys. D: Appl. Phys.* **35** 3181
- [14] Li H P, Pfender E and Chen Xi 2003 *J. Phys. D : Appl. Phys.* **36** 1084
- [15] Swank W.D, Fincke J R, Haggard D C, Sampath S and Smith W in : C.C.Berndt (Ed.), *Thermal Spray: A united forum for scientific and Technological Advances*, Published by ASM International, Ohio, USA, 1997, p.451
- [16] Wan Y P, Gupta V, Deng Q, Sampath S, Prasad V, Williamson R and Finke J R 2001 *J. Thermal Spray Techn.* **10** 382
- [17] Westhoff R and Szekely J 1991 *J. Appl. Phys.* **70** 3455

- [18] Chen Xi and Pfender E 1982 *Plasma Chem. Plasma Process.* **2** 185
- [19] Pfender E and Lee Y C 1985 *Plasma Chem. Plasma Process.* **5** 211
- [20] Vardelle A, Fauchais P, Dussoubs B and Themelis N J 1998 *Plasma Chem. Plasma Process.* **18** 551
- [21] Leylavergne M, Dussoubs B, Vardelle A and Goubot N 1998 *J. Thermal Spray Technol.* **7** 527-36
- [22] Ramachandran K and Nishiyama H 2004 *Thin Solid Films* **457** 158
- [23] Jenista J, Heberlein J V R and Pfender E 1997 *IEEE Trans. Plasma Sci.* **25** 883
- [24] Amakawa T, Jenista J, Heberlein J and Pfender E 1998 *J. Phys. D: Appl. Phys.* **31** 2826
- [25] McKelliget J W, Trapaga G, Gutierrez-Miravete E, and Cybulski M in: C.Coddet (Ed.), Proceeding of the 15<sup>th</sup> International Thermal Spray Conference, Nice, France, May 25-29, 1998, p.335.
- [26] Ramachandran K and Nishiyama H 2002 *J.Phys. D: Appl. Phys.* **35** 307
- [27] Ramachandran K and Nishiyama H 2003 *Thin Solid Films* **435** 298
- [28] Mostafa A A, and Mongia H C 1988 *Int. J. Heat Mass Transfer* **31** 2063
- [29] Pfender E 1989 *Plasma Chem. Plasma Process* **9** 167S